Langmuir
Article
pubs.acs.org/Langmuir

Influence of Salts and Natural Organic Matter on the Stability of Bacteriophage MS2

Steven E. Mylon,[†] Claudia I. Rinciog,[†] Nathan Schmidt,[‡] Leonardo Gutierrez,[§] Gerard C. L. Wong,[‡] and Thanh H. Nguyen*[,§]

[†]*Department of Chemistry, Lafayette College, Easton, Pennsylvania 18042,* [‡]*NSF Science and Technology Center for Water Purification, Department of Material Science and Engineering, University of Illinois, 205 North Mathews Avenue, Urbana, Illinois 61801, and* [§]*NSF Science and Technology Center for Water Purification, Department of Civil and Environmental Engineering, University of Illinois, 205 North Mathews Avenue, Urbana, Illinois 61801*

Received June 25, 2009. Revised Manuscript Received August 24, 2009

The stability of functionalized nanoparticles generally results from both steric and electrostatic interactions. Viruses like bacteriophage MS2 have adopted similar strategies for stability against aggregation, including a net negative charge under natural water conditions and using polypeptides that form loops extending from the surface of the protein capsid for stabilization. In natural systems, dissolved organic matter can adsorb to and effectively functionalize nanoparticle surfaces, affecting the fate and transport of these nanoparticles. We used time-resolved dynamic light scattering to measure the aggregation kinetics of a model virus, bacteriophage MS2, across a range of solution chemistries to determine what factors might destabilize viruses in aquatic systems. In monovalent electrolytes (LiCl, NaCl, and KCl), aggregation of MS2 could not be induced within a reasonable kinetic time frame, and MS2 was stable even at salt concentrations greater than 1.0 M. Aggregation of MS2 could be induced in divalent electrolytes when we employed Ca^{2+}. This trend was also observed in solutions containing 10 mg/L Suwannee River organic matter (SROM) reference material. Even at Ca^{2+} concentrations as high 200 mM, diffusion-controlled aggregation was never achieved, demonstrating an additional barrier to aggregation. These results were confirmed by small-angle X-ray scattering experiments, which indicate a transition from repulsive to attractive interactions between MS2 virus particles as monovalent salts are replaced by divalent salts.

1. Introduction

Viruses represent an important class of pathogenic nanoparticles in aquatic systems that are responsible for the vast majority of water-borne diseases. Because of this, viruses pose a challenge in removal and disinfection processes for drinking water suppliers. In environmental engineering, common means of disinfection have been chemical transformations and filtration. Only recently have studies focused on the importance of biophysical interactions between viruses and interfaces[1−3] which can be exploited as a method of disinfection or virus removal.

In the field of environmental engineering and science, the usual starting point for describing interfacial interactions of environmental nanoparticles is classical Derjaguin−Landau−Verwey−Overbeek (DLVO) theory that quantifies the balance between van der Waals interactions and electrostatic interactions. With the exception of a few cases,[4] DLVO theory on its own is insufficient and often requires extensions to include contributions from other interactions like Lewis acid−base interactions or steric interactions.[5] As a first approximation, the interfacial interactions of spherical virus nanoparticles such as bacteriophage MS2 have been modeled within the DLVO paradigm when modeling deposition of virus to mineral surfaces,[3] and DLVO-like interactions have also been successful in describing bacteriophage PRD1.[6] However, the complex interactions implicit in these systems often cannot be described using such models. For example, simple implementations of DLVO cannot adequately model microbial interactions at solid interfaces because of the heterogeneous polymer layers extending from cell membranes where synergistic combinations of steric and electrosteric interactions must be invoked.[7,8] Despite recent advances in describing the electrostatics of viruses and microorganisms by accounting for electrophoretic softness of these particles by Duval et al.,[9] it is clear that their structural complexities severely complicate exacting quantitative models describing interfacial interactions. In many cases, an appropriate electrostatic model is probably not enough. For example, using the total interaction energy profile for deposition of virus onto flat plates as a baseline model, Penrod et al.[10]needed to apply expressions for steric interaction energies that consisted of both a repulsive osmotic energy term to account for the water exclusion around polymers protruding from the virus surface and a repulsive elastic energy that is due to the compression of these polymers and their loss of configurational entropy.

*To whom correspondence should be addressed.

(1) Langlet, J.; Gaboriaud, F.; Gantzer, C.; Duval, J. F. L. *Biophys. J.* **2008**, *94* (8), 3293–3312.
(2) Langlet, J.; Gaboriaud, F.; Duval, J. F. L.; Gantzer, C. *Water Res.* **2008**, *42* (10−11), 2769–2777.
(3) Yuan, B. L.; Pham, M.; Nguyen, T. H. *Environ. Sci. Technol.* **2008**, *42*(20), 7628–7633.
(4) Chen, K. L.; Elimelech, M. *Langmuir* **2006**, *22*(26), 10994–11001.
(5) Grasso, D.; Subramaniam, K.; Butkus, M.; Strevett, K.; Bergendahl, J. *Rev. Environ. Sci. Bio/Technol.* **2002**, *1*, 17–38.
(6) Loveland, J. P.; Ryan, J. N.; Amy, G. L.; Harvey, R. W. *Colloids Surf., A* **1996**, *107*, 205–221.
(7) Walker, S. L.; Hill, J. E.; Redman, J. A.; Elimelech, M. *Appl. Environ. Microbiol.* **2005**, *71*(6), 3093–3099.
(8) Chen, G. X.; Walker, S. L. *Langmuir* **2007**, *23*(13), 7162–7169.
(9) Duval, J. F. L.; Busscher, H. J.; van de Belt-Gritter, B.; van der Mei, H. C.; Norde, W. *Langmuir* **2005**, *21*(24), 11268–11282.
(10) Penrod, S. L.; Olson, T. M.; Grant, S. B. *Langmuir* **1996**, *12*(23), 5576–5587.

In a more general context, DLVO theory itself is an approximation not intended for universal application. Within the paradigm of DLVO, one considers only electrostatic and van der Waals interactions and treats these interactions as if they were separable and, moreover, expresses each of these interactions in an approximate form. The mean field description of electrostatics implicit in DLVO cannot treat systems with strong electrostatic interactions (such as high surface charge densities and multivalent ions).[11−16] In such systems, effects from ion correlations, for example, can lead to counterintuitive phenomena such as like-charge attraction in polyelectrolytes,[17−19] as well as some of the intervirus interactions described here. A number of helpful reviews have recently been published.[20−23]

Several recent studies have demonstrated the importance of electrostatic interactions in the specific situation of adsorption of viruses to solid interfaces. For deposition of MS2 onto both bare silica and organic matter-coated silica, Yuan et al.[3] showed that an increasing ionic strength resulted in increasing deposition rates due to the high degree of charge screening. Additionally, Herath et al.[24] showed that as the pH of a solution approached the isoelectric point (IEP) of specific viruses, microfiltration membranes rejected a greater percentage of virus particles in solution. The authors speculated that this phenomenon was probably due to a higher degree of virus−virus aggregation resulting from weakened electrostatic interactions at the IEP. By measuring decreases in the mean apparent diffusion coefficient of virus suspensions with decreasing pH values using dynamic light scattering (DLS), Langlet et al.[2] confirmed that virus−virus aggregation resulted from decreases in the strength of electrostatic repulsive interactions as the IEP of the virus was approached.

On the basis of the research described above, we hypothesize that factors beyond electrostatics can influence virus−virus interactions and affect aggregation. These factors might include changes in ionic strength, the presence of multivalent cations, and in natural aquatic systems the presence of natural organic matter (NOM). For example, previous studies have shown multivalent cations can induce nonspecific attractions between like-charged polyelectrolytes such as DNA,[25−27] and filamentous phages,[19] and for F-actin, the structure and dynamics of the condensing ions have been directly investigated.[17,18] Furthermore, deposition of microbes onto solid interfaces can be enhanced in the presence of divalent cations due in part to cation bridging of extracellular polysaccharide polymers or charge neutralization through cation complexation to carboxylate functionalities.[4,8,28] To effectively determine the solution conditions and their degree of influence on the stability of the bacteriophage, MS2, sensitive time-resolved dynamic light scattering (TR-DLS) is an appropriate experimental method. By employing TR-DLS, we studied the aggregation kinetics of dilute MS2 suspensions under different experimental conditions. In other research, TR-DLS has been employed to measure the aggregation kinetics of suspensions such as metal oxide nanoparticles,[28−30] fullerenes,[4] and other important nanoparticles.[31] With state-of-the-art instrumentation, the small size of MS2 and the low solution concentrations do not pose a problem for detection or for resolving kinetics within the appropriate temporal window. On the basis of the results from these studies, the mechanism of aggregation can be postulated and the appropriate model for describing particle−particle interaction can be suggested. Inclusive with this TR-DLS study is the complementary synchrotron-based small angle X-ray scattering (SAXS) experimental results of MS2 suspensions over a range of solution conditions. On the basis of these sensitive studies, the second osmotic virial coefficient of MS2 at different solution chemistries can be determined, providing us with a clear indication of the conditions under which attractive or repulsive forces dominate virus−virus interactions.

The objective of this paper is to study a broad range of environmental factors that control the stability of MS2 in aquatic systems and compare those results against conventional descriptions for particle interaction. To this end, we investigated the influence various cations have on the stability of both bare MS2 and MS2 coated with SROM. Particle stability measurements commonly require measurements of particle aggregation that occurs when interactions become attractive. However, the appearance of aggregation does not need to be coincident with the onset of attractions. To examine the onset of attractive interactions between virus particles, we use synchrotron-based small-angle X-ray scattering to quantitatively measure the transition from repulsive to attractive interactions between MS2 particles, as specific solution conditions are systematically varied. The results of this prototypical system will inform our understanding of the complex balance of interactions (electrostatic, van der Waals, and steric interactions) responsible for controlling virus stability in aquatic systems.

2. Materials and Methods

2.1. MS2 Preparation and Plaque Forming Unit (PFU) Assay. Bacteriophage MS2 was replicated and purified following a modified procedure of Kitis et al.[32] A tryptic soy broth solution (TSB) was prepared via addition of 3 g of TSB to 100 mL of deionized water (18.2 MΩ cm DI, Millipore) and later autoclaved. *Escherichia coli* cells were grown in this TSB solution as its culture medium for approximately 3 h under incubation conditions (37 °C). The *E. coli* suspension was inoculated with MS2 when the optical density reached 1.0 at 420 nm. The solution was further incubated under the same conditions for an additional 24 h. For purification of MS2, the viral solution was centrifuged to separate

(11) Rouzina, I.; Bloomfield, V. A. *Biophys. Chem.* **1997**, *64*, 139–155.
(12) Golestanian, R.; Kardar, R.; Liverpool, T. B. *Phys. Rev. Lett.* **1999**, *82*(22), 4456–4459.
(13) Grønbech-Jensen, N.; Mashl, R. J.; Bruinsma, R. F.; Gelbart, W. M. *Phys. Rev. Lett.* **1997**, *78*, 2477–2480.
(14) Guldbrand, L.; Nilsson, L.; Nordenskiöld, L. *J. Chem. Phys.* **1986**, *85*, 6686–6698.
(15) Shklovskii, B. I. *Phys. Rev. Lett.* **1999**, *82*, 3268–3871.
(16) Rouzina, I.; Bloomfield, V. A. *J. Phys. Chem.* **1996**, *100*(23), 9977–9989.
(17) Angelini, T. E.; Liang, H.; Wriggers, W.; Wong, G. C. L. *Proc. Natl. Acad. Sci. U.S.A.* **2003**, *100*(15), 8634–8637.
(18) Angelini, T. E.; Golestanian, R.; Coridan, R. H.; Butler, J. C.; Beraud, A.; Krisch, M.; Sinn, H.; Schweizer, K. S.; Wong, G. C. L. *Proc. Natl. Acad. Sci. U.S.A.* **2006**, *103*(21), 7962–7967.
(19) Butler, J. C.; Angelini, T. E.; Tang, J. X.; Wong, G. C. L. *Phys. Rev. Lett.* **2003**, *91*, 028301.
(20) Wong, G. C. L. *Curr. Opin. Colloid Interface Sci.* **2006**, *11*, 310–315.
(21) Levin, Y. *Rep. Prog. Phys.* **2002**, *65*(11), 1577–1632.
(22) Holm, C. P. K.; Podgornik, R. *Electrostatic effects in soft matter and biophysics*; Kluwer: Dordrecht, The Netherlands, 2001.
(23) Gelbart, W. M.; Bruinsma, R. F.; Pincus, P. A.; Parsegian, V. A. *Phys. Today* **2000**, *53*(9), 38–44.
(24) Herath, G.; Yamamoto, K.; Urase, T. *Water Sci. Technol.* **1999**, *40*(4−5), 331–338.
(25) Livolant, F.; Leforestier, A. *Prog. Polym. Sci.* **1996**, *21*(6), 1115–1164.
(26) Raspaud, E.; Chaperon, I.; Leforestier, A.; Livolant, F. *Biophys. J.* **1999**, *77* (3), 1547–1555.
(27) Purdy Drew, K.; Sanders, L. K.; Culumber, Z. W.; Zribi, O.; Wong, G. C. L. *J. Am. Chem. Soc.* **2009**, *131*(2), 486–493.
(28) Chen, K. L.; Mylon, S. E.; Elimelech, M. *Environ. Sci. Technol.* **2006**, *40*(5), 1516–1523.
(29) Chen, K. L.; Mylon, S. E.; Elimelech, M. *Langmuir* **2007**, *23*(11), 5920–5928.
(30) Mylon, S. E.; Chen, K. L.; Elimelech, M. *Langmuir* **2004**, *20*(21), 9000–9006.
(31) Schudel, M.; Behrens, S. H.; Holthoff, H.; Kretzschmar, R.; Borkovec, M. *J. Colloid Interface Sci.* **1997**, *196*, 241–253.
(32) Kitis, M.; Lozier, J. C.; Kim, J. H.; Mi, B. X.; Marinas, B. J. *J. Am. Water Works Assoc.* **2003**, *95*(12), 105–119.

viruses from larger *E. coli* cellular debris. The supernatant was collected and filtered using a 0.2 μm low-protein binding track-etched polycarbonate membrane (Whatman Nucleopore) to remove material larger than 200 nm. Following this, an additional filtration step was conducted using a 0.05 μm low-protein binding track-etched polycarbonate membrane (Whatman Nucleopore) for removal of smaller particles. The resulting filtrate contained MS2, nutrients, microbial products, and very small debris, and this was removed by ultrafiltration. For ultrafiltration, a 100 kDa membrane was used in conjunction with a Millipore ultrafiltration unit. This unit was continuously fed with a previously filtered and autoclaved 1.0 mM NaCl solution with a 5:1 ratio of NaCl solution to viral solution. The viral suspension was therefore purified when all the contaminants smaller than ~100 kDa were removed through the membrane while the viruses were concentrated inside the unit. A laminar flow hood was used to prevent contamination at every step of the process.

MS2 enumeration was performed following the double-agar layer procedure.[33] For each sample taken, successive dilutions were prepared to produce a quantifiable solution. The Petri dishes were incubated at 37 °C for 16 h, and the plaques formed due to the inoculation of MS2 on *E. coli* were counted in every dilution. Only the samples that had from 20 to 300 plaques were finally taken into consideration for PFU determination.

All MS2 solutions used in subsequent experiments were created from concentrated stock solutions (ca. 10^{12} PFU/mL for DLS measurements and ca. 10^{15} PFU/mL for the SAXS measurements). For studies in the absence of NOM, MS2 stock solutions were prepared at pH 5.5 ± 0.2. For the studies on the effects of natural organic matter on MS2 stability, MS2 stock solutions were added to a solution of Suwannee River organic matter purchased from the International Humic Substance Society (IHSS, St. Paul, MN). All SROM solutions were doubly filtered through 0.2 μm syringe filters (Whatman). The concentrations of SROM solutions expressed as milligrams of organic carbon (OC) per liter were determined via high-temperature oxidation (Shimadzu 5000). Suspensions of SROM-coated MS2 were allowed to equilibrate at pH 4.8 ± 0.2 for a minimum of a couple of hours. The differences in pH for bare MS2 suspensions and SROM-coated MS2 suspensions were chosen for the maintenance of a constant eletrophoretic mobility of the particles between solution conditions.

2.2. Electrophoretic Mobility Measurements. The electrophoretic mobilities of the MS2 nanoparticles were measured with a Malvern Instruments Zetasizer-ZS (Malvern Instruments). Solutions of nanoparticles (ca. 10^{11} PFU/mL) were prepared at the appropriate ionic strength and titrated with aqueous NaOH made from a standardized solution (Aldrich) and filtered through a 0.2 μm syringe filter (Whatman) to remove any dust or particulates that might interfere with these measurements. Titrations were performed using a Malvern Instruments MPT-2 autotitrator, and measurements were taken using a folded capillary cell (Malvern Instruments). Titrations covered a range from pH 3 to 12 with measurements taken at increments of roughly 0.5 pH unit. The isoelectric point is defined in this work as the pH at which the electrophoretic mobility is zero. Electrophoretic mobility was measured at different pH values in solution with a fixed ionic strength of 1 mM.

2.3. Calcium Titration of SROM and MS2. Titration of SROM from the IHSS was conducted by the addition of a Ca^{2+} standard solution to suspensions of SROM that had been prepared as discussed above. As a control, titration of filtered DI water by Ca^{2+} was first conducted. The volume of DI water tested was 150 mL at an initial pH of ~5.9. The calcium concentration in solution was measured using a calcium combination electrode (Denver Instruments, catalog no. 0222617). From the manufacturer's specifications, the detection limit of this electrode ranged from 0.02 to 40000 ppm (5×10^{-7} to 1 M). Titration was conducted by the addition of a 0.001 M Ca^{2+} standard. The solution was continuously stirred, and the electrode response was recorded after the solution was stabilized with the addition of the titrant (~20 s). Two measurements were taken after each addition of Ca^{2+} to the solution (0.1−0.5 mL) and averaged prior to data reduction. The titration was ended when the Ca^{2+} concentration of the solution was ~0.00015 M. For the sake of completeness, the titration of SROM was conducted in solutions with different TOC concentrations (5, 12.5, 25, and 37.5 mg/L). A second set of experiments for SROM titration and control experiment was conducted following the same protocol described above, but with previous degassing of DI water with N_2 for 30 min prior to SROM solution preparation. A third set of experiments for SROM titration was conducted following the procedure described above, but with the addition of KCl at a final concentration of 20 mM for the purposes of ionic strength. MS2 was titrated with Ca^{2+} following the procedure described above. The concentrations of MS2 for the two conditions tested were 2.1×10^{12} and 1.1×10^{12} PFU/mL in 30 mL of solution.

2.4. Aggregation Kinetics Experiments. We employed a single-detector light scattering unit (ALV-CGS-3, Langen) to make all DLS measurements. The ALV-CGS-3 compact goniometer system employs a 22 mW HeNe laser (Uniphase) providing a single-frequency output with a wavelength of 632.8 nm, an ALV-proprietary optical fiber-based detector, and an avalanche photodiode single-photon detector. Samples were held in a thermostated index matching quartz vat filled with toluene doubly filtered through 0.02 μm filters (Anotop 25, Whatman). The sample temperature was ca. 22 °C but more importantly never varied by more than 0.5 °C during one run.

Borosilicate culture tubes (Fisher) where used as sample cuvettes. Prior to any experiments, the cuvettes were soaked in cleaning solution (Extran MA01, Merck) overnight, rinsed with DI water (18.2 MΩ, US Filter Purelab Plus), and dried in an oven before use. A new cuvette was used for each DLS measurement. All sample preparation took place in a class 100 trace metal clean vertical laminar flow hood (Air Clean Products 600). For sample preparation, the MS2 stock solutions were diluted to the appropriate concentration (ca. 10^{10} to 10^{11} PFU/mL) with 0.2 μm doubly filtered DI water and adjusted to the required pH with 0.2 μm filtered NaOH or HCl.

To induce aggregation, the appropriate amount of electrolyte stock solution, filtered with 0.1 μm filters (Anotop-25, Whatman), was added to the vial containing a known volume (ca. 1.0 mL) of MS2 sample. The solution was given a brief shake and quickly inserted into the index matching vat. Dynamic light scattering measurements were started immediately. The time required for the first DLS measurement was generally less than 15 s and was accounted for during data reduction.

Time-resolved dynamic light scattering was used to measure the intensity of the autocorrelation function of dilute virus nanoparticle suspensions at varying ionic compositions employing both monovalent (NaCl, LiCl, and KCl) and divalent ($CaCl_2$) electrolytes over a range of concentrations. All light scattering measurements were conducted by employing the detector positioned at a scattering angle of 90° from the incident laser beam. The detector signal was fed into the correlator, which accumulated each autocorrelation function for 5−15 s. The intensity-weighted hydrodynamic radius of the nanoparticle aggregates was calculated by nonlinear least-squares fitting of the second-order cumulants (ALV software). The measurements were performed over time periods from 10 min to 14 h because appropriate analysis of time-resolved DLS data requires approximately a 30% increase in the hydrodynamic radius.[4,28] This provides adequate data for derivation of the aggregation kinetics of doublet formation since the effective doublet hydrodynamic radius has been reported to be ~1.4 times the primary particle hydrodynamic radius.

(33) Adams, M. *Bacteriophages*; Interscience Publishers: New York, 1959.

2.5. Light Scattering Data Reduction. Initial nanoparticle aggregation kinetics were determined by monitoring the increase in R_H with time:[30,31]

$$\left(\frac{dR_H}{dt}\right)_{t\to 0} \propto k_{11}N_0 \quad (1)$$

That is, the product of aggregation rate constant k_{11} and nanoparticle number concentration N_0 is proportional to the slope of the R_H versus time graph for $t \to 0$. After the initial slope had been normalized to nanoparticle concentration, the inverse stability ratio ($1/W$) can be determined from the ratio of the measured aggregation rate constant, k, to the maximum aggregation rate constant, k_{fast}:

$$\frac{1}{W} = \frac{k}{k_{fast}} \quad (2)$$

As shown in earlier papers,[30,34] we can determine $1/W$ without determining the absolute rate constants, because the ratio of the initial slope of the R_H versus time graph to that in the fast regime is proportional to k/k_{fast}:

$$\frac{1}{W} = \frac{\left(\frac{dR_H}{dt}\right)_{t\to 0}}{\left(\frac{dR_H}{dt}\right)_{t\to 0:fast}} \quad (3)$$

The attachment efficiency, α, otherwise known as the inverse stability ratio, $1/W$, is used to quantify the aggregation kinetics of colloidal systems. Attachment efficiencies are calculated by normalizing the measured k_{11} by the diffusion-limited aggregation rate constant $(k_{11})_{fast}$ determined under favorable aggregation conditions.[30]

$$\alpha = \frac{k_{11}}{(k_{11})_{fast}} \quad (4)$$

The attachment efficiency α, ranging from 0 to 1, is the probability of an irreversible attachment resulting from the collision of two colloidal particles.

2.6. Small-Angle X-ray Scattering. MS2 stock solutions were prepared as described above. For SAXS experiments, samples were prepared over the MS2 concentration range of 0.5−16 mg/mL, or 7.9×10^{13} to 2.5×10^{15} PFU/mL. $CaCl_2$ concentrations of 1−50 mM (Aldrich) were selected to determine the salt concentration necessary to induce a net attractive MS2 interaction. NaCl (Aldrich) concentrations with the same ionic strength were prepared to investigate the effect of salt valence. All samples were titrated to pH 6.1 in 1 mM NaCl (Aldrich) . Samples were hermetically sealed in 1.5 mm diameter quartz capillaries. To minimize path length differences due to capillary size polydispersity, capillaries with the same thickness were chosen after measurement using a Nikon Eclipse E600 POL light microscope at 4× magnification.

Small-angle X-ray scattering experiments were performed on beamline 4-2 at the Stanford Synchrotron Research Facility (Palo Alto, CA) and beamline 12-ID-Cat at the Advanced Photon Source (Argonne, IL). For the Stanford Synchrotron Research Facility experiments (incident X-ray wavelength $\lambda = 1.1271$ Å), the scattered radiation was collected using a MAR Research (Evanston, IL) charge-coupled device (CCD) camera (pixel size of 79 μm × 79 μm). For the Advanced Photon Source experiments (incident X-ray wavelength $\lambda = 1.033$ Å), the scattered intensity was collected using a MAR Research 2D mosaic CCD detector (pixel size of 79 μm × 79 μm).

2.7. SAXS Data Reduction. Similar second virial coefficient measurements using X-rays have been conducted on DNA[35] and lysozyme[36] in salt solutions. Following these methods, we extrapolate the low-Q region [$Q = (4\pi/\lambda)\sin\theta$, where λ is the incident X-ray wavelength and 2θ the scattering angle] of the small-angle diffraction spectra to the origin ($Q = 0$) to obtain the second osmotic virial coefficient, A_2. A_2 is the first-order correction to the van't Hoff law [$\Pi/cRT = 1/M + A_2\rho = ...$ (terms of order ρ^2), where Π is the osmotic pressure, c is the MS2 concentration in grams per cubic centimeter, R is the ideal gas law constant, M is the molecular weight of MS2, and T is the absolute temperature]. Therefore, the osmotic pressure can be higher or lower than the ideal case, signifying a net repulsion or attraction between particles, respectively.

Experimentally, A_2 can be measured with X-rays since the X-ray structure factor at the origin is related to the osmotic pressure by the relationship $S(c, Q = 0) = (RT/M)(\partial\Pi/\partial c)^{-1}$, where $S(c, Q = 0)$ is the interparticle correlation function. This in conjunction with the van't Hoff law gives

$$\frac{P(Q=0)}{I(c,Q=0)} = \frac{1}{S(c,Q=0)} = 1 + (2MA_2)c \quad (5)$$

where $P(Q = 0)$ is the intraparticle form factor and $I(c, Q = 0)$ is the [MS2]-normalized measured scattering intensity extrapolated to the origin. Typically, the form factor which is proportional to the Fourier transform of the particle electron density is difficult to model. However, via comparison of SAXS spectra from samples with different particle concentrations under identical solution conditions [the same $P(Q)$], the nature of the interparticle interaction can be determined by the change in the low Q scattering intensity. For attraction (repulsion) between particles, $A_2 < 0$ ($A_2 > 0$), which implies the low Q scattering intensity, $I(c, Q = 0)$, will increase (decrease) with an increasing particle concentration.

3. Results and Discussion

3.1. Electrokinetic Measurements. The electrophoretic mobilities of the bare MS2 and SROM-coated MS2 nanoparticles as a function of ionic strength were used to calculate the outer surface potentials and electrophoretic softness using Ohshima's equation[37] for soft particles . For solutions containing Na^+ as a supporting electrolyte (Figure 1a), the electrophoretic mobilities of bare MS2 and SROM-coated MS2 became less negative with an increasing ionic strength. This result is due to a higher degree of screening of the applied electric field associated with the greater concentration of dissolved ions. In both cases, screening becomes limited at high ionic strengths, resulting in electrophoretic mobilities asymptotically approaching a finite lower limit. This limiting behavior results from an outer soft ion-permeable polymeric layer attached to the core shell of the MS2 and the SROM-coated MS2 nanoparticles.[1,37] Fits to Ohshima's equation were obtained for electrophoretic mobility data only at ionic strengths above 10 mM with the fixed charge density and electrophoretic softness used as fitting parameters. The electrophoretic softness, $1/\lambda$, is described in terms of length units where $\lambda = (\gamma/\eta)^{1/2}$ and γ is the frictional coefficient of the soft layer.[37] For bare MS2 in Na^+, $1/\lambda = 2.3$ nm, and for SROM-coated MS2, $1/\lambda = 2.6$ nm, confirming a greater depth of polyelectrolyte layer imparted to the MS2 nanoparticles by any additional SROM moieties adsorbed to the surface.

When the electrophoretic mobilities of MS2 and SROM-coated MS2 were measured in the presence of Ca^{2+} (Figure 1 b), the electrophoretic mobilities reached zero at ca. 200 mM Ca^2.

(34) Saleh, N. B.; Pfefferle, L. D.; Elimelech, M. *Environ. Sci. Technol.* **2008**, *42* (21), 7963–7969.

(35) Qiu, X.; Andresen, K.; Kwok, L. W.; Lamb, J. S.; Park, H. Y.; Pollack, L. *Phys. Rev.* **2007**, 99.

(36) Bonnete, F.; Finet, S.; Tardieu, A. *J. Cryst. Growth* **1999**, 196.

(37) Ohshima, H. *Colloids Surf., A* **1995**, *103*(3), 249–255.

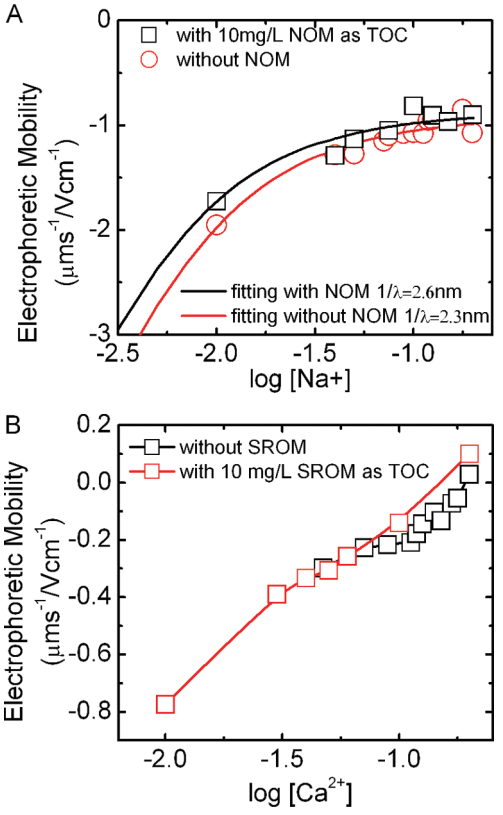

Figure 1. (a) Electrophoretic mobility as a function of ionic strength for MS2 in solution with and without SROM (10 mg/L as TOC). The electrophoretic mobility data were fitted with Ohshima's equation for outer surface potential and particle softness ($1/\lambda$). The solid lines in panel a represent the best fit where $1/\lambda = 2.3$ nm for bare MS2 and $1/\lambda = 2.6$ nm for SROM-coated MS2. (b) Electrophoretic mobility as a function of Ca^{2+} concentration for MS2 in solution with and without SROM. Lines are for guides only and do not represent a fit to a model prediction.

We hypothesize that this is due to a combination of charge screening by the divalent cations and complexation of Ca^{2+} to carboxylate moieties common to both the outer protein capsid of MS2 and the SROM.[1] Complementary titration data using a calcium ion-selective electrode (ISE) support this hypothesis as we observed small deviations in the ISE signal when Ca^{2+} was added to MS2 or SROM-coated MS2 suspensions.

3.2. Stability of MS2 and SROM-Coated MS2 in the Presence of Monovalent Salts. We examined the stability of MS2 and SROM-coated MS2 in solutions of monovalent salts LiCl, NaCl, and KCl over a range from 10 mM to 1.0 M. Initial concentrations of virus nanoparticles ranged from 5×10^9 to 5×10^{11} PFU/mL. For particles of the same radius, the diffusion-controlled rate constant for monomer−/monomer aggregation $k_{11} = 8k_BT/3\eta$, where η is the solution viscosity and k_BT is the product of the solution temperature and Boltzman's constant. For aqueous solutions at 25 °C, the theoretical diffusion-controlled rate constant for MS2−MS2 aggregation is 1.23×10^{-17} m^3/s. On the basis of this and the integrated second order rate equation, the theoretical half-life for aggregation of virus monomers within the diffusion-controlled limit is ca. 37 s at an initial virus concentration of 5×10^9 PFU/mL and 0.37 s at an initial virus concentration of 5×10^{11} PFU/mL. At the lowest salt concentrations, we did not expect to observe diffusion-controlled aggregation and therefore chose particle concentrations so that we could observe an appreciable degree of aggregation ($R_t = 1.4R_0$) within a reasonable temporal window. We considered a suspension stable if we could not observe aggregation under our experimental conditions within a reasonable time frame.

We observed some small changes in the initial hydrodynamic radius of MS2 and SROM-coated MS2 resulting from initial salt concentrations. At the lowest salt concentrations, the hydrodynamic radius for SROM-coated MS2 was 18.1 ± 0.7 nm and that of bare MS2 16.2 ± 0.1 nm, further indicating that the SROM was adsorbing to the surface of the MS2 nanoparticles. With increasing salt concentrations, we observed a decrease in the initial hydrodynamic radius for both sets of particles. Limiting hydrodynamic radii of 14.0 ± 0.1 and 14.5 ± 0.4 nm for MS2 and SROM-coated MS2, respectively, were observed at ionic strengths above 500 mM. This decrease in R_H with an increase in salt concentration is due to screening of charged moieties within the MS2 phage itself and the SROM polyelectrolyte. The effect has also been documented by Rotureau et al.,[38] who observed increases in the diffusion coefficients for functionalized carboxymethyldextran macromolecules with an increasing ionic strength. Despite changes in the initial hydrodynamic radius with an increasing ionic strength over the range of monovalent salt concentrations that we employed, the hydrodynamic radius for the particles measured at the beginning of each aggregation experiment was equal to that at the end of each experiment within experimental uncertainty. This is compelling evidence for the superior stability of these virus nanoparticles. In fact, additional laboratory experiments showed suspensions of MS2 nanoparticles (1×10^{12} PFU/mL) in ≤1.0 M NaCl were stable against aggregation for as much as 10 h.

In the case of conventional small particles destabilized through increases in ionic strength, we expect to see increasing rates of aggregation until diffusion-limited aggregation occurs. Within the paradigm of DLVO theory, a rough measure of aggregation tendency is given by the ionic strength at the crossover concentration to diffusion-limited aggregation. This is commonly termed the critical coagulation concentration (CCC) and results from screening of electrostatic interactions to a point where at the Debye length the balance of electrostatic repulsion forces and attractive van der Waals forces equals zero. Under these schematic conditions, a potential energy barrier to aggregation no longer exists and each collision between virus monomer nanoparticles results in the formation of a dimer aggregate. From the experimental results in monovalent salts up to the extremely high concentrations that we employed and within our generous temporal window, no CCC exists for MS2 and SROM-coated MS2, indicating that simple DLVO theory is inadequate for modeling virus−virus interactions. The failure of DLVO theory to effectively model MS2 interfacial interactions is not surprising in light of the surface charge heterogeneities associated with the protein capsid. One additional intriguing possibility for the superior stability of MS2 and SROM-coated MS2 in monovalent salt solutions originates from steric interactions between MS2 and SROM-coated MS2 particles. This is supported by the experimentally determined softness layer of 2.3 and 2.8 nm for MS2 and SROM-coated MS2, respectively. These steric interactions arise from polypeptides that form loops at the capsid surface and have been implicated in influencing the filtration of MS2.[10]

3.3. Aggregation of MS2 and SROM-Coated MS2 in the Presence of Ca^{2+}. With the addition of $CaCl_2$ to aqueous suspensions of MS2 and SROM-coated MS2 under the same experimental conditions that we employed for the monovalent salts, we were able to observe aggregation of the virus

(38) Rotureau, E.; Thomas, F.; Duval, J. F. L. *Langmuir* **2007**, *23*(16), 8460–8473.

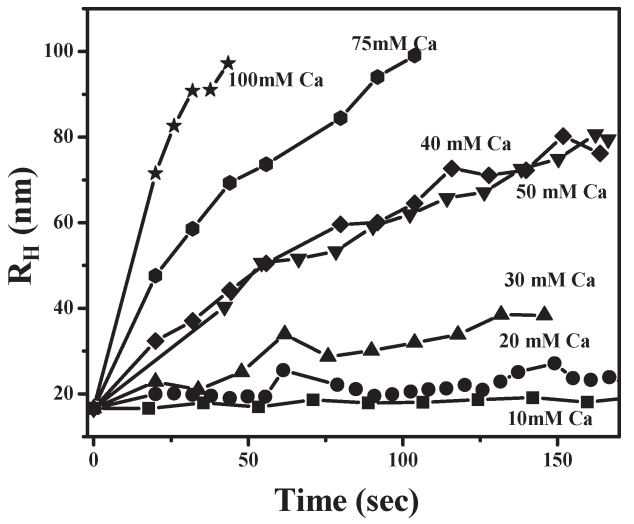

Figure 2. Typical results from multiple TR-DLS experiments for MS2 in a $CaCl_2$ solution in the presence of 10 mg/L SROM (as TOC).

nanoparticles. Figure 2 shows a set of representative data from a series of aggregation experiments for SROM-coated MS2. The growth rate of the MS2 aggregates increases with an increasing $CaCl_2$ concentration following typical nanoparticle aggregation behavior observed previously.[29,39]

Panels a and b of Figure 3 show plots of the log of the inverse stability ratio as a function of the log.[40] For both MS2 and SROM-coated MS2, there are clear delineations between the regions of favorable and unfavorable aggregation and the CCCs for these suspensions are ca. 160 and 100 mM Ca^{2+}, respectively. We do note the calculated aggregation rate constants at the CCC for both of these systems are below the theoretical diffusion-controlled aggregation rate constant, but this has been observed before for a similar experimental protocol.[29] Despite the fact that Ca^{2+} ions were able to induce aggregation, the observed CCCs for both systems are quite large compared to those from similar experiments examining other types of nanoparticles and therefore again indicate a significant degree of stability for MS2 suspensions.

On the basis of these results, Ca^{2+} ions appear to have a substantial effect on destabilization of the SROM-coated MS2 and uncoated MS2 compared to monovalent cations. A similar, albeit more dramatic, effect of Ca^{2+} ions on the aggregation behavior of other nanoparticles has been observed by Chen et al.[39] In their work, complexation of calcium to the high-molecular weight organic polyelectrolyte, alginate, resulted in enhanced aggregation of hematite nanoparticles. Enhanced aggregation described aggregation that appeared to exceed the theoretical diffusion-controlled limit; this would be predicted when calcium cross-linking of alginate molecules formed a superstructure instead of conventional aggregates. Calcium titration experiments with SROM in our laboratory indicated a weak complexation of Ca^{2+} by SROM similar to that found by Hering and Morel.[41] Additionally, molecular modeling supports the experimental evidence that Ca^{2+} forms complexes with natural organic matter.[40,42] In light of the low organic matter concentrations used

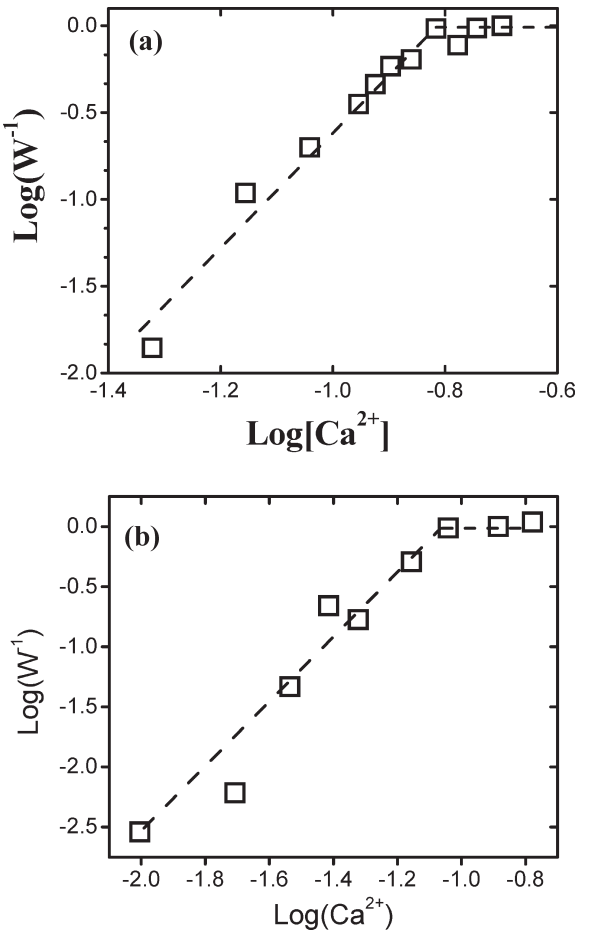

Figure 3. (a) Stability diagram for bare MS2 in a $CaCl_2$ solution at 295 K. [MS2] = 8.2×10^{10} PFU/mL. (b) Stability diagram for MS2 in a $CaCl_2$ solution in the presence of 10 mg/L SROM (as TOC) at 295 K. [MS2] = 8.2×10^{10} PFU/mL.

in our experiments, we do not expect Ca^{2+} to have contributed to any substantive cross-linking of SROM molecules. We propose that the mechanism for virus aggregation in the presence of Ca^{2+} ions involves charge neutralization and cation bridging due to complexation of Ca^{2+} to negatively charged moieties on the MS2 surface. This is further supported by calcium titrations to MS2 suspensions in which we did observe calcium complexation. A small additional degree of complexation to the SROM may indeed result in the minor differences in CCCs observed for the two suspensions because complexation by Ca^{2+} can lower the overall surface charge and destabilize the virus nanoparticle. Alternatively, complexation by Ca^{2+} may also induce changes in the MS2 capsid which can affect important structural characteristics such as polypeptide loops that would be responsible for the steric stabilization of MS2 particles against aggregation. Given the weak stability constants for complexation of Ca^{2+} to MS2 that our titrations predict, either of these two mechanisms might be responsible for MS2 aggregation and both are supported by the high concentrations of Ca^{2+} that are required. The same effect caused by structural changes may occur as the IEP of MS2 is approached and may be responsible for aggregation of MS2 in these cases as well.[2,24] Structural changes of this nature might be difficult to show given the difficulty in imaging MS2 at a sufficiently high resolution. However, studies such as this are necessary for the development of a clearer understanding of the mechanism of MS2 aggregation.

(39) Chen, K. L.; Mylon, S. E.; Elimelech, M. *Enivron. Sci. Technol.* **2006**, *40*, 1516–1523.
(40) Ahn, W. Y.; Kalinichev, A. G.; Clark, M. M. *J. Membr. Sci.* **2008**, *309* (1−2), 128–140.
(41) Hering, J. G.; Morel, F. M. M. *Environ. Sci. Technol.* **1988**, *22*(10), 1234–1237.
(42) Kalinichev, A. G.; Kirkpatrick, R. J. *Eur. J. Soil Sci.* **2007**, *58*(4), 909–917.

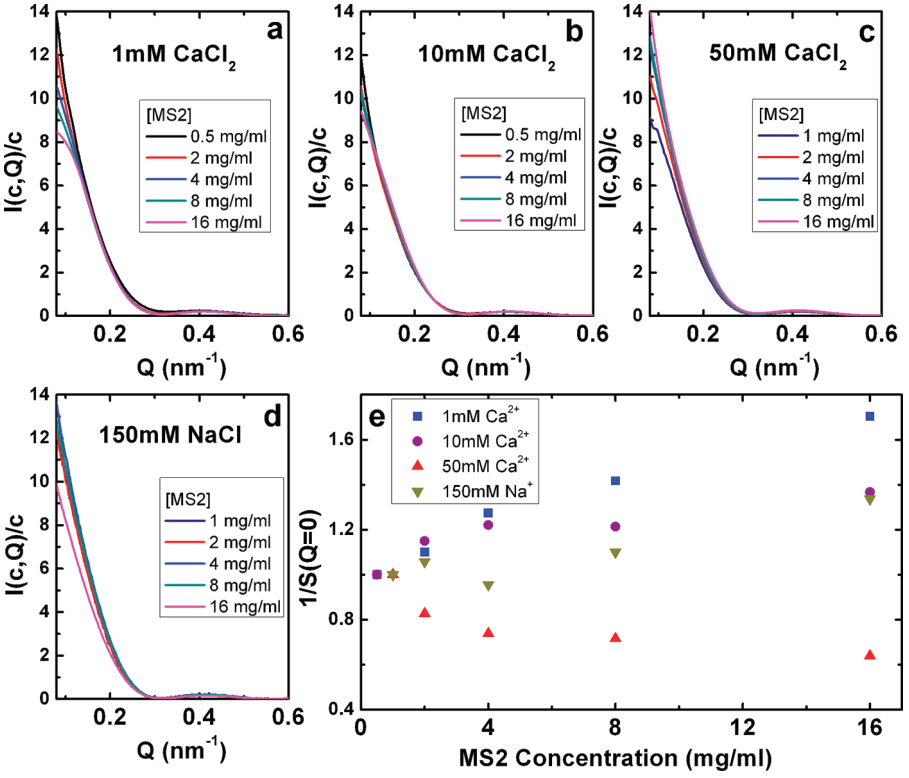

Figure 4. (a−e) Experimentally measured SAXS intensities for MS2 in Ca^{2+} and Na^{+} salt solutions (a−d). A downturn in the low-Q scattering profile with an increasing MS2 concentration implies inter-MS2 repulsion (a, b, and d), whereas an upturn (c) implies attraction. (e) Resulting $1/S(Q = 0)$ vs [MS2] for a given salt solution after extrapolation to obtain $I(c, Q = 0)$. The experimentally determined A_2 values are extracted through a linear fit using eq 5. $A_2 = 2.34 \times 10^{-6}$ mol mL g^{-2} for 150 mM NaCl and 6.41×10^{-6}, 3.51×10^{-6}, and -3.88×10^{-6} mol mL g^{-2} for 1, 10, and 50 mM $CaCl_2$, respectively.

3.4. Synchrotron-Based Small-Angle X-ray Scattering. Small-angle X-ray scattering results confirm the existence of a net attractive interaction between MS2 nanoparticles, with an onset at high concentrations of Ca^{2+}. For 1 and 10 mM Ca^{2+} (Figure 4a,b), there is a downturn in the spectra with an increase in particle concentration. This is the scattering signature for the existence of a net repulsive interaction and shows that such repulsions are present at low divalent salt concentrations. The trend is reversed for 50 mM Ca^{2+} (Figure 4c). The upturn observed for concentrations greater than 50 mM Ca^{2+} is the signature for attractive interactions and indicates that higher calcium concentrations induce a net attraction between particles. The importance of cation valence is apparent from comparison with NaCl salt solutions. Unlike the 50 mM Ca^{2+} which shows an upturn with an increase in particle concentration signifying attraction, NaCl with the same ionic strength still displays a downturn implying marginally repulsive behavior between MS2 particles.

Quantitatively, $I(c, Q = 0)$ can be obtained by extrapolation of the low-Q (Guinier) region which is well described by $I(c, Q) = I(c, 0)e - (QR_g)^{2/3}$, where R_g is the particle electric radius of gyration. Therefore, analysis reduces to a linear fit of $\ln[I(c, Q)]$ versus q^2 to yield the intensity at the origin. By approximation of the scattering intensity from the spectra with the lowest concentration to be dominated by the particle form factor, i.e., $S(c_{min}, Q) = 1$, the second virial coefficient, A_2, can be obtained using eq 5. In this case, a positive slope indicates repulsion while a negative slope indicates attraction.

As predicted by qualitative inspection of the SAXS data, quantitative analysis confirms that increasing the divalent calcium concentration decreases the level of interparticle repulsion (Figure 4e), and above a threshold concentration, the interaction becomes attractive. At 50 mM Ca^{2+}, $A_2 < 0$, showing this calcium concentration is sufficient to induce a net attraction between the negatively charged MS2. This is close to the same concentration at which aggregation was observed in the TR-DLS experiments but below the CCC. Thus, by combining DLS with synchrotron X-ray scattering, two techniques which measure different aspects of the same phenomena at different length scales, we are able to show that the existence of an attractive interaction does not imply aggregation and that there is a finite threshold of attraction strength before the onset of aggregation.

When the interactions of MS2 are compared in monovalent salts, even at 150 mM Na^{+} the slope remains positive, indicating a repulsive regime persists up to this sodium concentration. This result confirms the superior stability of MS2 nanoparticles in the presence of high concentrations of monovalent cations.

4. Conclusions

Here we investigated how solution conditions influence the interfacial interactions of bacteriophage MS2 and contribute to MS2 aggregation in aquatic systems. As MS2 captures the essential characteristics of many infectious virus particles, its aggregation is important to understand fully, especially since the aggregation of pathogens may change both their infectivity and filtration efficiency. While others have reported that the protonation of acid functionalities that are associated with MS2 results in a decrease in surface charge and subsequent MS2 aggregation at the IEP, this is the first study to compare contributions from monovalent and divalent cations as well as organic matter.

Above the MS2 IEP at high concentrations of monovalent salts where the Debye layer becomes less than 1 nm thick, electrostatic repulsion between surface charges cannot be effective in stabilizing MS2 solutions against aggregation; however, MS2 nanoparticles are kinetically inert against aggregation, and the second osmotic virial coefficient remains positive for MS2 suspensions. While the patchiness of surfaces charges may result in strong localized regions of surface charge that might still stabilize MS2 particles even at high IS, on the basis of the crystal structure of MS2, we speculate that structural features such as polypeptide loops that extend from the protein capsid also contribute to the stabilization of MS2 against aggregation through steric interactions. The strength of these steric interactions probably depends on many factors such as the surface density of the functionality, the length of the functionality, and whether that functionality is charged. For example, hematite nanoparticles functionalized with a humic acid standard were also stabilized against aggregation due to steric and electrosteric interactions,[30] but aggregation in these system could still be induced by simply adding more salt to the solutions. The results presented here indicate that this is not the case for MS2, and therefore, the unique stability of MS2 is probably due to a more uniform distribution of functionalities on the protein capsid when compared to humic acid standards adsorbed to the surface of a metal oxide nanoparticle. In fact, our results indicate that OM slightly destabilizes MS2 in the presence of Ca^{2+} probably because it provides more functionalities with which Ca^{2+} can form a complex, potentially altering the structure of the moieties responsible for stabilizing the virus. Considering that MS2 virus nanoparticles are replicated within a bacteria cell where the relative ionic strength is already fairly high, the necessity of these structural features seems clear. Without them, MS2 might aggregate irreversibly within the bacteria host and therefore would be unable to propagate to infect others.

The situation in the presence of the divalent cations is more complicated. As in the case of monovalent salts, aggregation of MS2 is not observed until comparatively high concentrations of salt are used. Our recent work focusing on deposition of MS2 on environmental surfaces under environmentally relevant conditions with a Ca^{2+} concentration of < 1 mM[43] found no aggregation was observed with such a low Ca^{2+} concentration. This is in agreement with our aggregation work presented here.

At higher Ca^{2+} concentrations, MS2 aggregation is observed using TR-DLS. Additionally, SAXS shows that the second osmotic virial coefficient turns negative at the highest concentrations of Ca^{2+}, indicating a crossover region from stable MS2 suspensions at low Ca^{2+} concentrations to unstable suspensions at higher concentrations. There are a number of possibilities for this that go beyond charge neutralization, including the existence of ion correlations that induce attractions, as well as potential structure changes in MS2 itself, induced by divalent cations.

Acknowledgment. We acknowledge the Lafayette College EXCEL scholars research program (C.I.R.) and NSF MRI Grant 0619409. We also thank Xiangyun Qiu for helpful comments regarding the second virial coefficient data analysis. This work was partially supported by the WaterCAMPWS, a Science and Technology Center of Advanced Materials for the Purification of Water with Systems under National Science Foundation Contract CTS-0120978, the Department of Civil and Environmental Engineering at the University of Illinois, USDA Grant 2008-35102-19143, and a Fulbright fellowship. Portions of this research were conducted at the Stanford Synchrotron Radiation Lightsource (SSRL), at the Advanced Photon Source (APS), and at the Fredrick Seitz Materials Research Laboratory (FS-MRL, Urbana, IL). The SSRL is a national user facility operated by Stanford University on behalf of the U.S. Department of Energy, Office of Basic Energy Sciences. The SSRL Structural Molecular Biology Program is supported by the Department of Energy, Office of Biological and Environmental Research, and by the National Institutes of Health, National Center for Research Resources, Biomedical Technology Program. Use of the Advanced Photon Source was supported by the U.S. Department of Energy, Office of Science, Office of Basic Energy Sciences, under Contract DE-AC02-06CH11357.

(43) Pham, M.; Mintz, E. A.; Nguyen, T. H. *J. Colloid Interface Sci.* **2009**, *338* (1), 1–9.